Measurement of aerodynamic coefficients of tower components of Tsing Ma Bridge under yaw winds

L. D. Zhu[†]

State Key Laboratory for Disaster Reduction in Civil Engineering, Tongji University, 1239 Siping Rd. Shanghai 200092, China

Y. L. Xu[†]

Department of Civil and Structural Engineering, The Hong Kong Polytechnic University, Hung Hom, Kowloon, Hong Kong, China

F. Zhang[‡] and H. F. Xiang[†]

Department of Bridge Engineering, Tongji University, 1239 Siping Rd., Shanghai 200092, China

Abstract. Tsing Ma Bridge in Hong Kong is the longest suspension bridge in the world carrying both highway and railway. It has two H-shape concrete towers, each of which is composed of two reinforced concrete legs and four deep transverse prestressed concrete beams. A series of wind tunnel tests have been performed to measure the aerodynamic coefficients of the tower legs and transverse beams in various arrangements. A 1:100 scaled 3D rigid model of the full bridge tower assembled from various tower components has been constructed for different test cases. The aerodynamic coefficients of the lower and upper segments of the windward and leeward tower legs and those of the transverse beams at different levels, with and without the dummy bridge deck model, were measured as a function of yaw wind angle. The effects of wind interference among the tower components and the influence of the bridge deck on the tower aerodynamic coefficients were also investigated. The results achieved can be used as the pertinent data for the comparison of the computed and field-measured fully coupled buffeting responses of the entire bridge under yaw winds.

Key words: Tsing Ma Bridge; tower leg; tower transverse beam; yaw wind; aerodynamic coefficient; wind tunnel test.

1. Introduction

With the increase in span length of the modern cable-supported bridges, the prediction of buffeting response of these bridges becomes more and more important. Accordingly, the buffeting analysis methods (Davenport 1962, Scanlan and Gade 1977, Scanlan 1978, Lin 1979, Lin and Yang 1983) have been continuously refined. Nowadays, multi-mode and inter-mode effects on

---

† Professor
‡ Senior Engineer

buffeting response can be included in either the time domain methods (Diana *et al.* 1998, Boonyapinyo *et al.* 1999, Chen *et al.* 2000a) or the frequency domain methods (Jain *et al.* 1996, Xu *et al.* 1998, Katsuchi *et al.* 1999, Chen *et al.* 2000b). Fully coupled 3D buffeting analyses, including not only the effects of inter-modes and multi-modes, but also the interaction among major bridge components, can also be performed using a combination of the pseudo-excitation method and the finite element (FE) approach (Xu *et al.* 2000). To have a more realistic comparison of the computed and field-measured buffeting responses of long span bridges, the frequency domain buffeting analysis method has been further refined to consider skew wind cases (Zhu *et al.* 2000, Zhu *et al.* 2001). In this refined method, the aerodynamic buffeting forces on bridge towers and the interaction between bridge deck and towers will be included in the buffeting analysis. The aerodynamic buffeting forces on a bridge tower will be detailed up to structural members such as tower legs and transverse beams. This treatment may be necessary for achieving a good comparison when the configuration of bridge tower is complex and the bridge is under yaw winds.

In this connection and to be consistent with wind tunnel tests for aerodynamic coefficients and flutter derivatives of the bridge deck under skew winds, as described in Zhu *et al.* (2001), this paper takes the Tsing Ma Bridge in Hong Kong as an example and presents a detailed wind tunnel investigation for determining the mean aerodynamic coefficients of the tower legs and transverse beams in various arrangements and under smooth flow condition. The effects of boundary layer turbulent flow on the aerodynamic force and hence aerodynamic behavior of the bridge are considered through the so-called aerodynamic admittance functions, as adopted by most of the traditional bridge buffeting analysis methods based on the quasi-steady theory. The effects of mean wind profile on the aerodynamic buffeting forces, and therefore the aerodynamic responses of the bridge tower, are naturally included in the refined method via the finite element method.

Though sectional model tests, using either pressure or force balance test technique, are often employed to measure the aerodynamic coefficients of bridge tower legs for its convenience and economy (Larose *et al.* 1993, 1995, Ricciardelli and Vickery 1994, 1998), the effect of the horizontal transverse beams of the tower and the effect of the bridge deck cannot be easily included. Also, as observed in both full-scale measurements (Larose *et al.* 1997) and wind tunnel tests (Ricciardelli and Vickery 1994, 1998), the aerodynamic interference between two tower legs may be significant. Furthermore, the cross section dimension of the lower segment of the Tsing Ma bridge tower leg below the bridge deck is significantly larger than that of the upper segment of the tower leg above the deck. Therefore, in this study, measurements of aerodynamic forces have been performed on the lower and upper segments of the windward and leeward tower legs and on the transverse beams at different levels, with and without dummy bridge deck model and for different yaw wind angles. The effects of aerodynamic interference among the tower components, and the influence of the bridge deck on the tower aerodynamic coefficients were also investigated.

2. Design of tower model

2.1. Tsing Ma Bridge Tower

The Tsing Ma Bridge has two H-shaped concrete towers: the east one is called the Tsing Yi tower and the west one is called the Ma Wan tower. Each tower is composed of two reinforced concrete legs and four deep transverse prestressed concrete beams (see Fig. 1). The two towers are almost identical. Therefore, only the Ma Wan tower was selected and tested in this study.
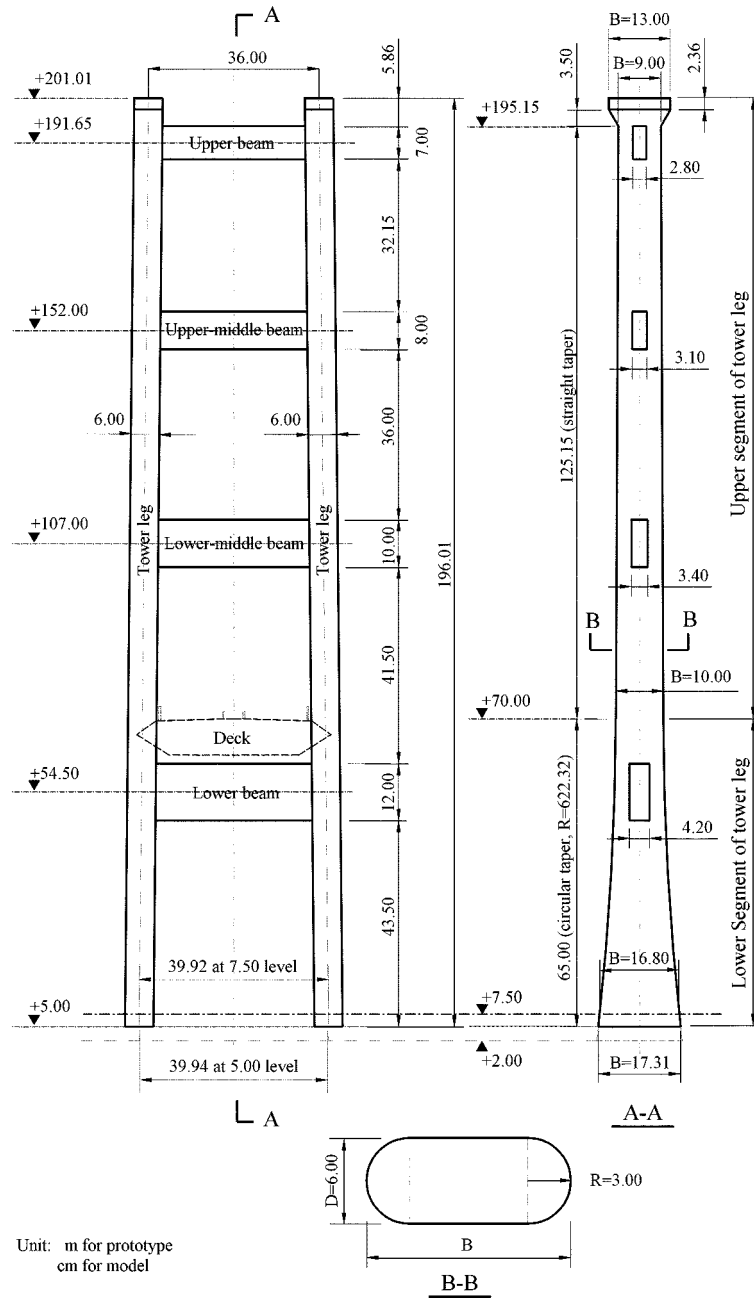
Fig. 1 Ma Wan Tower of Tsing Ma Bridge

The center-to-center distance of the two tower legs is 36.00 m at the top of the legs and 39.94 m at the base of the legs, resulting in a small taped angle of about 1%. The profile of the cross-section of the tower leg is composed of a central rectangle and two hemi-circles with a radius of 3.00 m. The radius of the hemi-circle is constant but the width of the rectangle varies along the height. With

reference to Section A-A of Fig. 1, the width B of the cross section of the tower leg is about 17.31 m at the base of the leg. It then tapers down to 10.00 m at a level of 70.00 m in circular curve on both sides of the leg with a radius of 622.32 m. It then further tapers down linearly to 9.00 m at the top face of the upper transverse beam. The width of the cross section finally increases linearly from 9.00 m to 13.00 m in the next 3.50 m and then keeps constant to the top of the leg. The depth D of the cross section of the tower leg, however, is constant and equal to 6.00 m along the height of the leg. All the transverse beams have a rectangular cross section. The lower transverse beam, just beneath the bridge deck, is 12.00 m high and 4.20 m wide, and the upper beam is 7.00 m high and 2.80 m wide. The lower-middle beam is 10.00 m in height and 3.40 m in width and the upper-middle beam is 8.00 m in height and 3.10 m in width.

2.2. Design of tower model

The tests were carried out in smooth flow in the TJ-2 Wind Tunnel of the State Key Laboratory for Disaster Reduction in Civil Engineering at Tongji University, People's Republic of China. The TJ-2 Wind Tunnel is a boundary layer tunnel of closed circuit type. The working section of the tunnel is 3.00 m wide, 2.50 m high, and 15.00 m long. The achievable mean wind speed ranges from 0.5 m/s to 68.0 m/s, and it is continuously adjustable.

According to the wind tunnel size, the geometrical scale of the Ma Wan tower was selected as 1:100. The tower was carefully modeled for its aerodynamics but the base line of the tower model was selected at a height of 7.50 m in the prototype tower (Figs. 1 and 2). The space between the levels of 5.00 m and 7.50 m in the prototype was then left in the model for installing an aluminum link between the base of the tower model and the force balance (see Fig. 2). As a result, the height of the tower model excluding the link was 1935.1 mm. The model was made of hard wood except that half of a perspex pipe of 30.0 mm radius was glued onto each side of the wood core to simulate the shape of the hemi-circle parts of the tower legs. The tower model was assembled from two tower legs and four transverse beams. A circular steel plate was fixed at the base of each leg. The diameter of the circular plate was 350.0 mm and its thickness was 5.0 mm. The two legs and the four transverse beams could be disconnected and remounted in different ways, depending on the test cases.

To consider the influence of the bridge deck on the wind flow around the bridge tower, a section
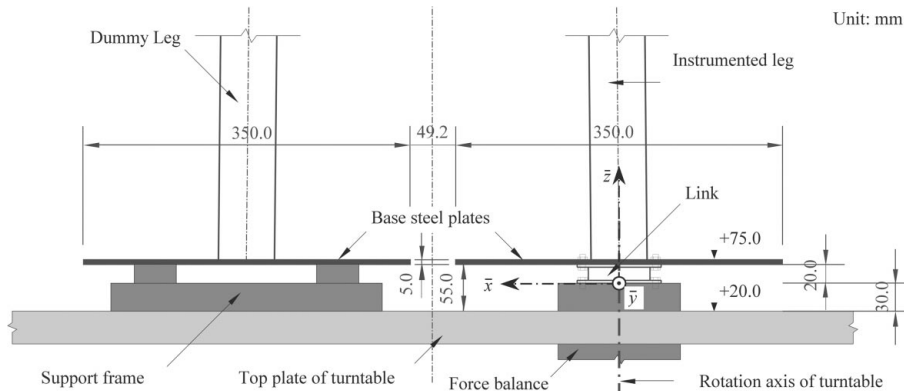

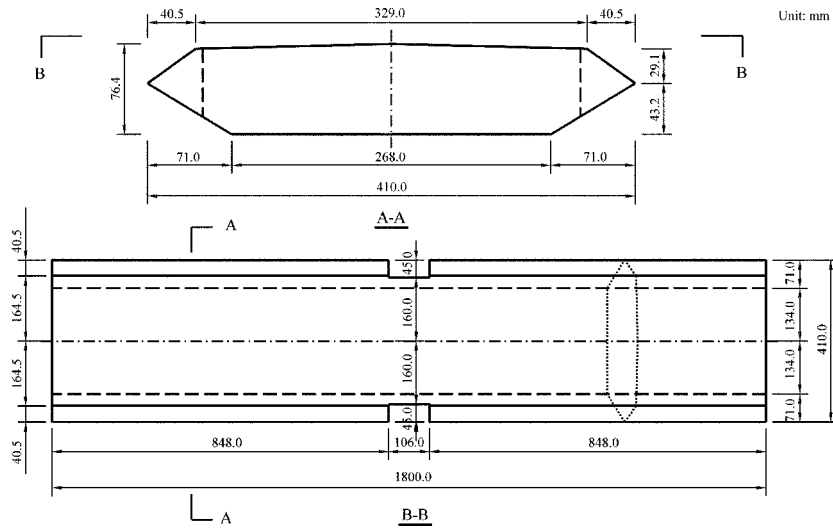Fig. 2 Schematic diagram of tower model installations

Fig. 3 Configuration and dimensions of the dummy deck model

equivalent to a 180.00 m long segment of the full-scale bridge deck was connected to the bridge tower. This section was considered to be a dummy deck model in the wind tunnel tests. The configuration and dimensions of the dummy model are shown in Fig. 3. The parapet and the windshield on the bridge deck were modeled but the central ventilation slots of the bridge deck were not included as the effects were considered to be small. The 1800.0 mm long dummy deck model was made of foam plastic and mounted on the tower model symmetrically with respect to the tower plane.

2.3. Test cases and model installation

There were a total of 9 cases considered in this wind tunnel investigation (see Table 1). In Case 1, the aerodynamic forces acting on one single tower leg were measured with the dummy deck, the dummy tower leg and the transverse beams in place. The four transverse beams were connected to the dummy tower leg, which was fixed to the top plate of the turntable. The instrumented tower leg was centrally mounted on a five-component force balance through the aluminum link (Fig. 2). The five-component force balance was vertically connected to the balance support post, which was firmly mounted at the center of the base plate of the turntable. The dummy deck model was symmetrically installed with respect to the tower, but it was fixed directly to the turntable through four vertical thin bars (Fig. 4). Small gaps of about 3 mm in width were left between the instrumented tower leg and the four transverse beams, and between the instrumented tower leg and the deck model.

In Cases 2 to 5, the aerodynamic forces acting on each transverse beam were measured with the dummy deck model in place. The measurement of aerodynamic forces on each transverse beam was indirect in this study. For example, to determine the aerodynamic forces on the upper transverse beam, the element was disconnected from the dummy tower leg and rigidly connected to the instrumented tower leg at the original level. The total aerodynamic forces acting on the instrumented tower components, including both the instrumented tower leg and the upper transverse beam, were

Table 1 Test cases for aerodynamic coefficients of Tsing Ma Bridge tower

Case	Instrumented component	Surrounding components	Range of β_T	Increment of β_T
1	One tower leg	One tower leg; 4 transverse beams; Deck segment	$0^o \sim 180^o$	3°
2	One tower leg; Upper transverse beam	One tower leg; Lower, lower-middle and upper-middle transverse beams; Deck segment	$0^o \sim 180^o$	3°
3	One tower leg; Upper-middle transverse beam	One tower leg; Lower, lower-middle and upper transverse beams; Deck segment	$0^o \sim 180^o$	3°
4	One tower leg; Lower-middle transverse beam	One tower leg; Lower, upper-middle and upper transverse beams; Deck segment	$0^o \sim 180^o$	3°
5	One tower leg; Lower transverse beam	One tower leg; Lower-middle, upper-middle and upper transverse beams; Deck segment	$0^o \sim 180^o$	3°
6	One tower leg	One tower leg; 4 transverse beams;	$0^o \sim 180^o$	6°
7	One tower leg	None	$0^o, 3^o, 6^o \sim 90^o$	6°
8	Lower segment of one tower leg	One tower leg; 4 transverse beams; Deck segment; Upper segment of instrumented leg	$0^o \sim 180^o$	3°
9	Lower segment of one tower leg	One tower leg; 4 transverse beams; Upper segment of instrumented leg	$0^o \sim 180^o$	6°

measured in a way similar to Case 1. The aerodynamic forces on the upper transverse beam were then calculated by the subtraction of the aerodynamic forces on the instrumented tower leg obtained in Case 1 from that obtained in the present case.

The aerodynamic forces acting on the instrumented tower leg without the dummy deck model in place were measured in Case 6. The comparison between the aerodynamic forces measured in Case 1 and Case 6 would reveal the influence of the presence of the dummy deck model. The aerodynamic forces acting on a single tower leg without any dummy models were measured in Case 7. In this case, the dummy tower leg and the four transverse beams in Case 6 were removed, leaving only one tower leg on the force balance. The influence of the dummy tower leg and the four transverse beams on the aerodynamic forces acting on the instrumented tower leg could be evaluated through the comparison between the aerodynamic forces measured in Case 6 and Case 7.

Considering the significant variation in width of the cross section of a tower leg from the base to an elevation of 70.00 m in full scale, the instrumented tower leg was thus further divided into two parts at a height of 700.0 mm in Case 8 and a small horizontal gap of about 3 mm was left between the upper and lower segments, as shown in Fig. 5. The upper segment was connected to the dummy tower leg, while the lower segment was mounted on the force balance. All other arrangements,
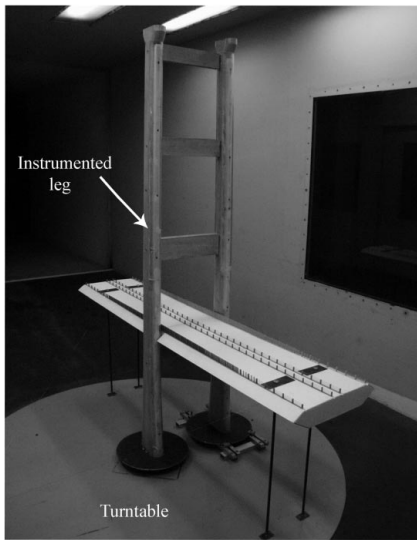
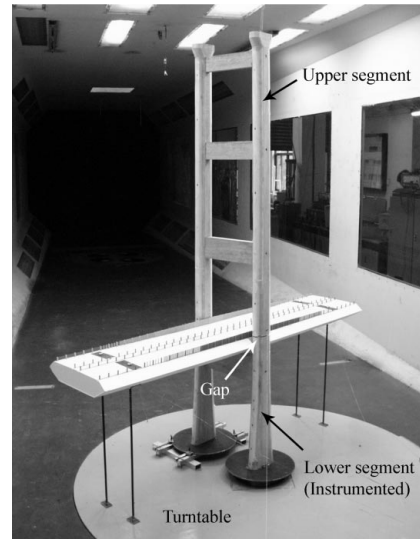Fig. 4 Entire leg measurement with bridge deck

Fig. 5 Lower leg segment measurement with bridge deck

including the four dummy transverse beams and the dummy deck model, were kept the same as those in Case 1. The aerodynamic forces on the lower segment of the tower leg were measured in this case. The aerodynamic forces on the upper leg segment were calculated by subtracting the aerodynamic forces on the lower segment measured in the present case from those on the entire leg measured in Case 1.

In the last case, i.e., Case 9, the aerodynamic forces on the lower segment of the tower leg without the deck influence were measured. After the aerodynamic forces on the lower segment had been measured, the aerodynamic forces on the upper segment of the tower leg without the deck influence were taken as the difference between the aerodynamic forces on the entire tower leg (measured in Case 6) and the aerodynamic forces on the lower segment (measured in Case 9).

3. Measurement system

The measurement system used in the wind tunnel tests for measuring the aerodynamic forces on the different structural components of the bridge tower was composed of a five-component force (moment) balance, a potentiostatic DC power supply (Ts1721), a multi-channel DC voltage amplifier (Ts3815T), a multi-channel data acquisition unit (HP3852A) and a computer (HP9000-345). The force balance test technique has the advantage of the pressure test technique for this study. This is because the cross section of the Tsing Ma bridge tower varies along the height, and the mean aerodynamic forces on the bridge tower components should be measured in various arrangements. The pressure measurement of a few sectional models of the bridge tower will be very difficult to fulfill this task, or it will be very expensive, if it is not impossible.

The five-component force balance used in these tests was a base-supported strain balance and met the requirements for high sensitivity and high stiffness, to avoid the model vibration and to ensure the measurement accuracy. Five groups of strain gauges were respectively stuck on three separated

sections of the balance, to measure two forces ($F_{\bar{x}}$ and $F_{\bar{y}}$) and three moments ($M_{\bar{x}}, M_{\bar{y}}$ and $M_{\bar{z}}$) with respect to the center of the balance at its top surface. The corresponding design bearing capacity was 100.0N and 200.0N, respectively, for two forces $F_{\bar{x}}$, $F_{\bar{y}}$, and 100.0 Nm, 50.0 Nm and 10.0 Nm, respectively, for three moments $M_{\bar{x}}, M_{\bar{y}}$ and $M_{\bar{z}}$. As shown in Fig. 2, $\bar{z}$ denotes the longitudinal (vertical) axis of the balance while $\bar{x}$ and $\bar{y}$ denote the two transverse (horizontal) axes, respectively, with the $\bar{x}$, $\bar{y}$ and $\bar{z}$ axes perpendicular to each other. In this investigation, the $\bar{x}$ axis is located in the tower plane and the $\bar{y}$ axis is along the bridge deck axis. The origin of the balance $\overline{xyz}$ coordinates is assigned at the center of the top surface of the balance.

4. Wind tunnel tests

All the 9 test cases listed in Table 1 were investigated for a series of wind directions, where the angle β_T represents the clockwise angle rotation of the turntable (see Fig. 6). In consideration of the symmetry of the bridge tower in its plane, the test range of β_T was from 0° to 180°. The yaw wind angle β_0 is defined as zero when the wind is normal to the longitudinal alignment of the bridge (see Fig. 6). The designated angle β_0 was then calculated from the angle β_T. In fact, when β_T varied from 0° and 90°, the instrumented tower leg was in windward position and $\beta_0=\beta_T$ ($\beta_0=0^o$ to 90°) for the windward tower leg (see Fig. 6a). When the angle β_T further increased from 90° to 180°, the instrumented tower leg was in leeward position and $\beta_0=\beta_T-180^o$ ($\beta_0=-90^o$ to 0°) for the leeward tower leg (see Fig. 6b). Because of the symmetry of the bridge tower, the aerodynamic coefficients of the windward tower leg for the yaw wind angle β_0 between -90° and 0° could be obtained from those of the windward tower leg measured for the angle β_0 between 0° and 90°, with the drag coefficient being symmetric and the lift coefficient being anti-symmetric. Similarly, the aerodynamic coefficients of the leeward tower leg for β_0 between 0° and 90° could be obtained from those measured for β_0 between -90° and 0°. For each test case, the measurements were repeated at least three times, and the average values would be presented. Based on some trial tests, the test mean wind speed was finally selected as 15 m/s. Each single measurement lasted for 10 seconds, with a sample frequency of 500 Hz. The time-averaged method was used to analyze the data to obtain the

(a) $0^o \leq \beta_T \leq 90^o$ (windward tower leg)   (b) $90^o \leq \beta_T \leq 180^o$ (leeward tower leg)
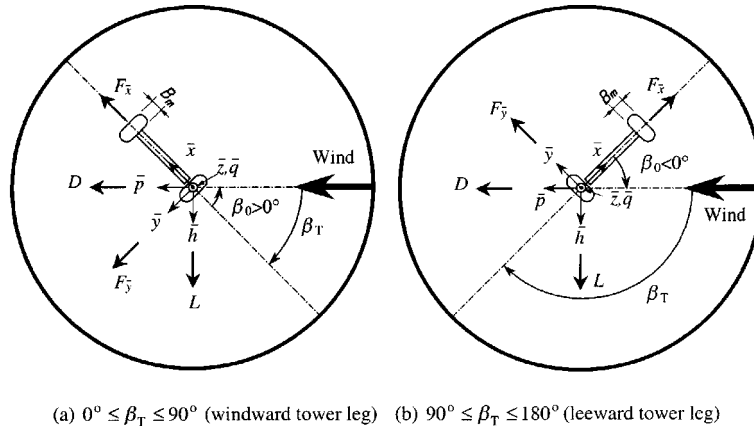
Fig. 6 Positive directions of aerodynamic forces on tower legs

mean aerodynamic coefficients. Since the blockage ratio, i.e., the projected area of the bridge tower model over the cross section of the wind tunnel, is less than 7.5%, no blockage corrections are applied to the results.

5. Calculation of aerodynamic coefficients

5.1. Drag and lift coefficients of tower leg

For the bridge tower leg, Fig. 6 shows the balance coordinates $\overline{xyz}$-system, and the wind coordinate $\overline{qph}$-system. In the $\overline{xyz}$-system originating at the center of the top surface of the balance and following the right-hand rule, the $\bar{z}$-axis is vertical, and the $\bar{x}$-axis and $\bar{y}$-axis are in the horizontal plane with the $\bar{x}$-axis in the tower plane. In the wind coordinates, the $\bar{q}$-axis is in the vertical direction, whilst the $\overline{h}$-axis and the $\bar{p}$-axis are in the horizontal plane with the $\bar{p}$-axis parallel to the mean wind direction.

Although the five aerodynamic forces/moments were measured on the tower leg, only the lift and drag forces are presented in this paper, because all the others were quite small and would not significantly affect the buffeting response of the whole bridge. The positive directions of the aerodynamic forces along the balance axes $\bar{x}$ and $\bar{y}$ ($F_{\bar{x}}$ and $F_{\bar{y}}$) and the lift (L) along the $\overline{h}$ axis and the drag (D) along the $\bar{p}$ axis are shown in Fig. 6a for the windward tower leg and in Fig. 6b for the leeward tower leg. Thus, the mean values of the lift and drag forces can be calculated from the measured mean aerodynamic forces using the following equations for both the windward and leeward tower legs.

$$L = -F_{\bar{x}}\sin\beta_T + F_{\bar{y}}\cos\beta_T \tag{1}$$

$$D = F_{\bar{x}}\cos\beta_T + F_{\bar{y}}\sin\beta_T \tag{2}$$

The average values of the drag and lift coefficients of tower legs are then determined as

$$C_D = 2D/(\rho\overline{U}_m^2 D_m L_m) \tag{3}$$

$$C_L = 2L/(\rho\overline{U}_m^2 D_m L_m) \tag{4}$$

where $\rho=1.225$ kg/m^3 is the air density; $\overline{U}_m$ is the test wind speed of 15 m/s; $D_m=0.06$ m is the depth of tower leg; L_m is the length of the tower leg segment: 1.31 m for the upper leg segment, 0.65 m for the lower leg segment and 1.96 m for the whole tower leg (including the aluminum link).

5.2. Coefficients of drag and crosswind force of tower transverse beam

Fig. 7a shows the balance coordinate $\overline{xyz}$-system, and wind coordinate $\overline{qph}$-system for the tower transverse beams for β_T from 0° to 90°, whilst Fig. 7b shows those for β_T from 90° to 180°. In the figures, $F_{\bar{x}}$ and $F_{\bar{y}}$ are the mean aerodynamic forces acting on the transverse beams along the $\bar{x}$ and $\bar{y}$ axes, respectively. These forces were obtained by the subtracting the aerodynamic forces on the instrumented tower leg obtained in Case 1 from the total aerodynamic forces obtained in one of Cases 2 to 5. D and C are the mean drag and crosswind forces along the wind $\bar{p}$ and $\bar{q}$ axes. These
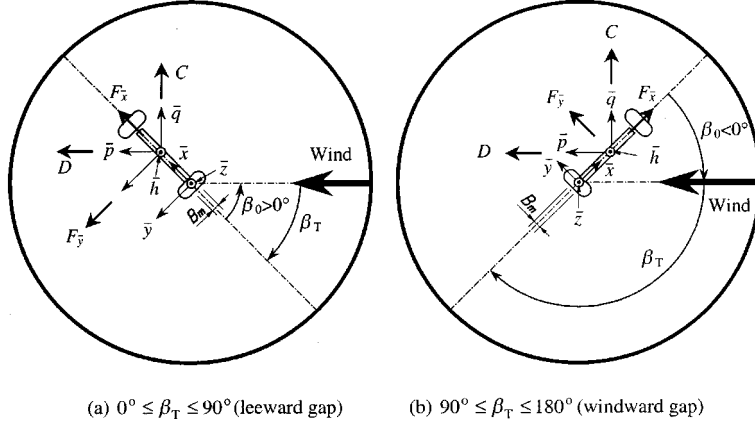
(a) $0^\circ \leq \beta_T \leq 90^\circ$ (leeward gap)　　(b) $90^\circ \leq \beta_T \leq 180^\circ$ (windward gap)

Fig. 7 Positive directions of aerodynamic forces on tower transverse beams

forces, as a function of wind yaw β_0 ranging from -90° to 90°, were then calculated as

$$D = F_{\bar{x}}\cos\beta_T + F_{\bar{y}}\sin\beta_T \tag{5}$$

$$C = F_{\bar{x}}\sin\beta_T - F_{\bar{y}}\cos\beta_T \tag{6}$$

The mean coefficients of drag and crosswind forces of the tower transverse beams were calculated as

$$C_C = 2C/\rho \bar{U}_m^2 B_m L_m \tag{7}$$

$$C_D = 2D/\rho \bar{U}_m^2 B_m L_m \tag{8}$$

where B_m and L_m are the width and length of the tower transverse beam, respectively. Here, B_m is 0.028 m, 0.031 m, 0.034 m, 0.042 m and L_m is 0.300 m, 0.307 m, 0.316 m, and 0.327 m for the upper, upper-middle, lower-middle and lower transverse beams, respectively.

6. Measurement results

The aerodynamic forces measured by the balance under designated wind directions were first analyzed to obtain the mean coefficients of the drag/lift/crosswind force of the tower members. These discrete mean coefficients were then interpolated using spline functions or fitted using polynomial functions to obtain the aerodynamic coefficient curves, which are presented and analyzed in this paper. It should be noted that all the coefficients provided here refer to the wind coordinate $\overline{qph}$-system.

6.1. Drag and lift coefficients of tower legs

The drag and lift coefficients of the windward and leeward entire legs of the Tsing Ma bridge tower, with and without the presence of the deck segment (Case 1 and Case 6) are shown in Figs. 8
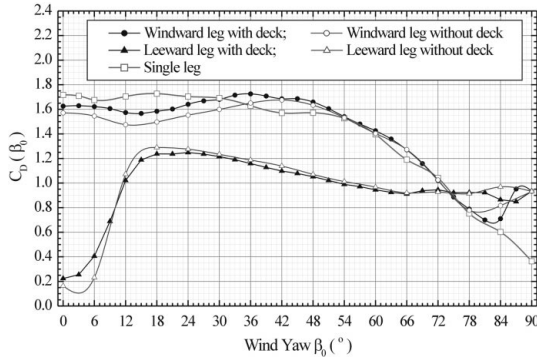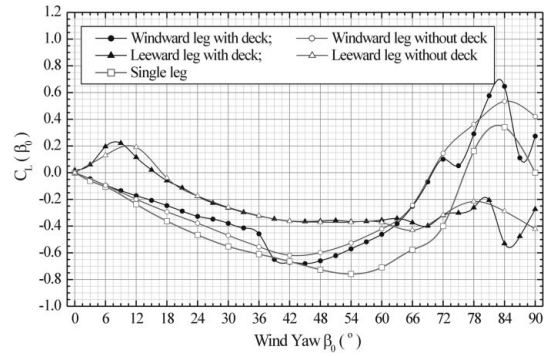
Fig. 8 Drag coefficients of tower legs

Fig. 9 Lift coefficients of tower leg

and 9 as a function of yaw wind angle β_0 from 0° to 90°. The drag and lift coefficients of the single tower leg without any dummy models in place (Case 7) are also plotted in Figs. 8 and 9. Based on these measured results, the following observations and comments are made.

6.1.1. Drag and lift coefficients of single tower leg

The drag coefficient of the single tower leg is about 1.7 and remains almost constant in the range of $0^o \leq \beta_0 \leq 30^o$, as shown in Fig. 8. This means that the drag coefficient of the single tower leg is not sensitive to yaw wind angle in this range. With further increase of yaw wind angle β_0, the drag coefficient of the single tower leg decreases. In particular, the drag coefficient decreases almost linearly with the angle β_0 when β_0 is larger than 55°. As shown in Fig. 9, the lift coefficient of the single tower leg is negative in the range of $0^o \leq \beta_0 \leq 76^o$ and becomes positive afterwards. The lift coefficient reaches its minimum value of -0.75 at β_0 of 54° and its maximum value of 0.35 at β_0 of 82°. Such variations of drag and lift coefficients are mainly attributed to the shape and size of the tower leg.

6.1.2. Drag and lift coefficients of windward tower leg

The drag coefficient of the windward tower leg with the dummy models of leeward tower leg and transverse beams, but without the dummy deck segment, is smaller than that of the single tower leg in the range of $0^o \leq \beta_0 \leq 36^o$, as shown in Fig. 8. The small reduction in the drag coefficient may be attributed to the obstruction of the transverse beams on the suction of leeward face of the windward tower leg. The drag coefficients of these two cases become similar for β_0 varying from 36° to 78°. After that (i.e., $\beta_0 > 78^o$), the drag coefficient of the windward tower leg is significantly larger than that of the single tower leg, as a result of the sudden change in the flow pattern.

With the addition of the dummy bridge deck segment, the drag coefficient of the windward tower leg is slightly larger, in the range of $0^o \leq \beta_0 \leq 40^o$, than that of the same tower leg without the dummy deck segment. The drag coefficients of these two cases are almost the same for β_0 varying from 40° to 80°. One may thus conclude that the interference effect from the deck segment on the drag coefficient of the windward tower leg is insignificant when $0^o \leq \beta_0 \leq 80^o$.

Compared with the lift coefficient of the single tower leg, the influence of the leeward leg and the transverse beams on the lift coefficient of the windward leg is relatively small when $\beta_0 < 42^o$, as shown in Fig. 9. This may happen because for small β_0 the leeward leg and the transverse beams could exert little influence on the flow patterns over the side faces of the windward tower leg. The difference between these two cases becomes remarkable when β_0 is larger than 42°, due to the interference with the transverse beams and leeward leg. Particularly, the lift force on the windward leg with the dummy models is not equal to zero when $\beta_0 = 90^o$.

With the dummy deck segment added to the model, the measured lift coefficients of the windward tower leg are quite different from those of the single tower leg in a wide range of yaw wind angle. However, if compared with the lift coefficient of the windward tower leg without the dummy deck segment, the presence of the dummy deck segment exerts relatively small influence on the lift coefficient in the range of $0^o \le \beta_0 \le 70^o$.

6.1.3. Drag and lift coefficients of leeward tower leg

Fig. 8 clearly demonstrates that the drag coefficient of the leeward tower leg with the dummy windward leg and transverse beams in place varies significantly from that of the single tower leg and that of the windward tower leg with the dummy models. For β_0 varying from 0° to 70°, the drag coefficients of the leeward leg are considerably smaller than those of the windward tower leg. This is mainly due to the sheltering effect from the windward tower leg and the transverse beams. The sheltering effect from the windward leg is particularly significant when β_0 is small so that the drag coefficient of the leeward leg is only about 0.2 compared with 1.7 for the single tower leg and 1.6 for the windward leg. The sheltering effect from the windward leg, however, decreases as β_0 increases. Though the transverse beams provide some sheltering effects on the leeward leg, they may also accelerate the wind flow about the leeward leg. More vortexes and hence turbulence may also be generated in the leeward face of the leeward leg because of the transverse beams, resulting in negative pressure area on the leeward face of the leeward leg. As a result of all these factors, the drag coefficient of the leeward leg suddenly increases from 0.2 to 1.3 when the yaw wind angle increases from 6° to 15°. It then reduces gradually down to 0.9 at $\beta_0 = 66^o$ and remains almost constant for larger yaw angles.

If compared to the drag coefficients of the leeward tower leg without the dummy deck segment, the drag coefficients of the leeward leg with the dummy deck segment are slightly higher when $0^o \le \beta_0 \le 8^o$, perhaps because of the increase of wind speed caused by the blockage of deck segment. Then, up to a value of $\beta_0 = 80^o$ the influence of the dummy deck segment on the drag coefficient of the leeward leg becomes insignificant.

By comparing the lift coefficients of the single tower leg and the leeward tower leg with the dummy models, one may see that the lift coefficients of the leeward tower leg with the dummy models vary significantly with β_0. In the range of $0^o \le \beta_0 \le 10^o$, the presence of the windward leg and transverse beams leads to an increase in the lift coefficients of the leeward leg. The lift coefficients of the leeward leg then decrease when β_0 increases from 10° to about 40°, but it is still larger than the lift coefficients of the windward tower leg. When β_0 further increases, the effect of the windward leg and the transverse beams makes the lift coefficients of the leeward leg not sensitive to β_0 up to a yaw angle of 70°. It is also noticed that when $\beta_0 = 90^o$, the presence of the transverse beams leads to the wind flow pattern to be asymmetric, generating a non-zero lift force on the leg. Similar to the drag coefficients, it is seen from Fig. 9 that the presence of the dummy

deck segment does not significantly affect the lift coefficients of the leeward tower leg except when the yaw wind angle is larger than 80°.

6.2. Drag and lift coefficients of upper and lower tower leg segments

Figs. 10 and 12 show the drag and lift coefficient curves of the upper segment of the windward and leeward tower legs with and without the presence of the deck segment, plotted as a function of yaw wind angle β_0 (Case 8 and Case 9). Figs. 11 and 13 show the corresponding curves for the lower segment.

6.2.1. Drag coefficients of upper and lower tower leg segments

It can be seen from Fig. 10 that the variation with yaw wind angle β_0 of drag coefficient of the upper segment of the windward leg is very similar to that of drag coefficient of the entire windward

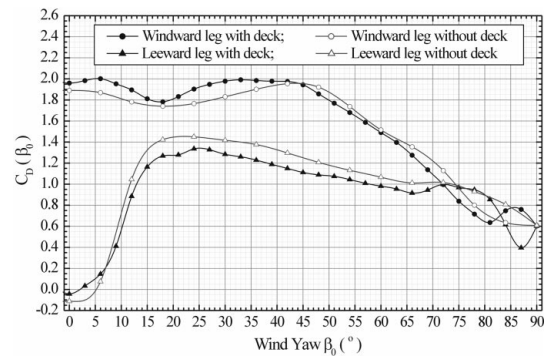Fig. 10 Drag coefficients of upper segment of tower leg

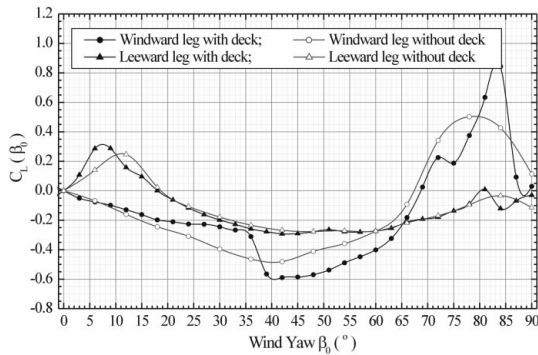Fig. 11 Drag coefficients of lower segment of tower leg

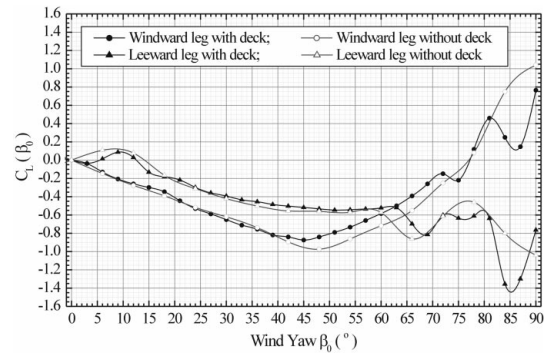Fig. 12 Lift coefficients of upper segment of tower leg

Fig. 13 Lift coefficients of lower segment of tower leg

leg shown in Fig. 8. The pattern of the drag coefficient of the lower segment of the windward leg (see Fig. 11) is, however, slightly different from that of the upper segment of the windward leg. The drag coefficient of the lower segment is larger than that of the upper segment when β_0 is less 75°. This is mainly because the exposed dimension of the lower segment is larger than that of the upper segment. Thus, it is necessary to take into account the different aerodynamic coefficients in the upper and lower leg segments in carrying out buffeting analysis for the whole bridge. The drag coefficient reaches the maximum value of about 1.6 for $\beta_0=36°$, for the upper segment, and the maximum values of about 2.0 for $\beta_0=36°$ and 6° for the lower segment.

For both the upper and lower windward leg segments, the presence of the dummy deck segment leads to a small increase in the drag coefficient of about 6% when $0° \leq \beta_0 \leq 40°$. This may be due to the presence of deck segment leading to an increase in local wind pressures on the windward leg. This small effect diminishes as β_0 becomes larger mainly because the deck dimension normal to wind direction reduces significantly. Nevertheless, the effect of the bridge deck on the drag coefficients of both upper and lower segments of the windward leg may be neglected.

The variation of drag coefficient of the upper segment of the leeward leg with β_0 is quite similar to that of drag coefficient of the entire leeward leg shown in Fig. 8. The variation of drag coefficient of the lower segment of the leeward leg with β_0 is also similar to that of drag coefficient of the entire leeward leg except for β_0 larger than 70°. The maximum value of the drag coefficient of the upper segment of the leeward leg is about 1.2 occurring for β_0 around 18° and that of the lower segment is about 1.3 occurring for β_0 around 24°. Nevertheless, the drag coefficients of both upper and lower segments of the leeward leg are significantly different from those of the upper and lower segments of the windward leg, respectively. Thus, it is necessary to distinguish the aerodynamic coefficients of the windward tower leg from those of the leeward tower leg.

The presence of the deck segment affects the drag coefficient of the upper segment of the leeward tower leg when $0° \leq \beta_0 \leq 10°$ (see Fig. 10). However, when β_0 is larger than 10°, this influence becomes insignificant. For the lower segment of the leeward leg, the presence of the bridge deck reduces the drag coefficient of about 10% when $10° \leq \beta_0 \leq 70°$ (see Fig. 11).

6.2.2. Lift coefficients of upper and lower tower leg segments

It can be seen from Fig. 12 that the lift coefficients of the upper segment of the windward tower leg, with and without the dummy deck segment, are very similar to those of the entire windward tower leg, shown in Fig. 9. The lift coefficients of the lower segment of the windward tower leg, however, are to a certain extent different from the above two cases. The lift coefficient decreases approximately linearly with the increase of β_0 up to 33° for the upper segment, and up to 45° for the lower segment. There is a sudden change in the lift coefficient of the upper segment of the windward leg with the dummy deck segment when β_0 is about 38°, but this does not occur for the lift coefficients of the lower segment of the windward leg.

Similar observations can be made for the upper and lower segments of the leeward tower leg with and without the dummy deck segment. The lift coefficients of the upper segment of the leeward leg, as shown in Fig. 12, are similar to those of the entire leeward leg shown in Fig. 9. The lift coefficients of the lower segment of the leeward leg, however, are different from the above two cases, in particular when β_0 is larger than 60°. This indicates that in the buffeting analysis of the Tsing Ma Bridge and in the comparison with the field measurement, it will be appropriate to use separate aerodynamic coefficients for the upper and lower segments of the windward and leeward
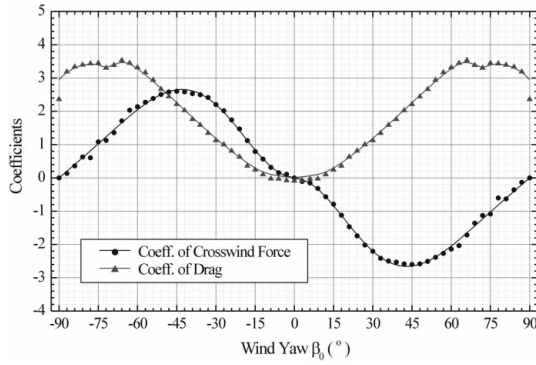
Fig. 14 Coefficients of drag and crosswind force of lower transverse beam
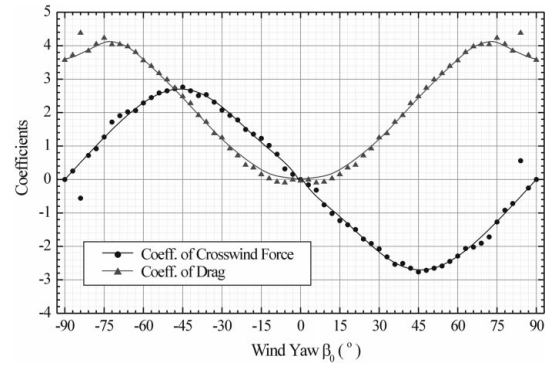

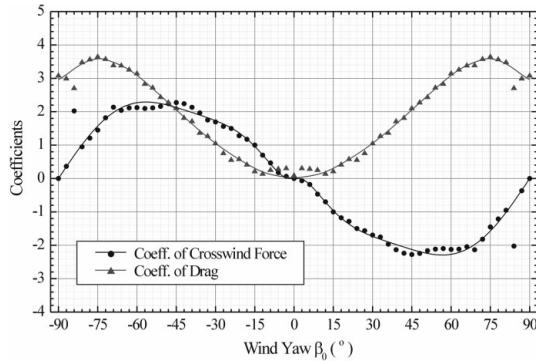Fig. 15 Coefficients of drag and crosswind force of lower-middle transverse beam

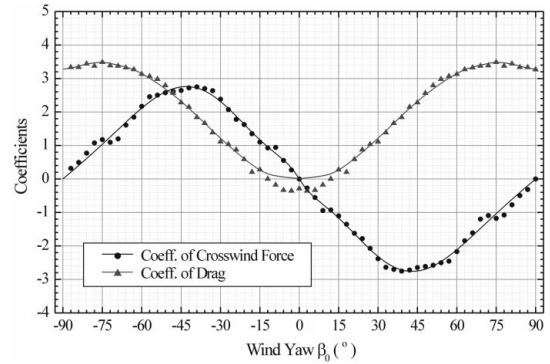Fig. 16 Coefficients of drag and crosswind force of upper-middle transverse beam

Fig. 17 Coefficients of drag and crosswind force of upper transverse beam

tower legs, rather than those of the tower as a whole.

6.3. Drag and crosswind force coefficients of transverse beams

The measured drag and crosswind force coefficients of the four transverse beams of the Tsing Ma bridge tower with the dummy deck segment are plotted in Figs. 14 to 17 respectively, as a function of yaw wind angle β_0. The measured data are fitted using polynomial functions, which are also shown in Figs. 14 to 17. The variations of both drag and crosswind force coefficients with β_0 are similar to each other for all the four transverse beams. The crosswind force coefficients vary with β_0 in a manner similar to a sine wave. The drag coefficients, however, seem to have the shape of a cosine wave but it is distorted in magnitude for $|\beta_0|$ ranging from 66° to 90° for the lower transverse beam and from 0° to 15° for the other three transverse beams. It is interesting to notice that such a distortion becomes weak for the upper transverse beam.

7. Conclusions

An extensive wind tunnel investigation has been performed to measure the aerodynamic coefficients of all the major structural members of the Tsing Ma bridge tower, to facilitate the fully coupled 3D buffeting analysis of the bridge and to understand the wind interference between the tower structural components. The following are major observations made from this investigation.

(1) The drag coefficients of the windward tower leg with the dummy leeward tower leg and four transverse beams have a slight difference from those of the single tower leg for most of the concerned yaw wind angles. The influence of the leeward leg and of the transverse beams on the lift coefficient of the windward leg is also relatively small when $\beta_0 < 42^o$, but becomes remarkable when β_0 is larger than 42°. The interference effect with the deck segment on both the drag and lift coefficients of the windward tower leg is insignificant in the range of $0^o \leq \beta_0 \leq 70^o$.

(2) The drag coefficients of the leeward tower leg with the dummy windward leg and transverse beams are significantly different from those of both the single tower leg and the windward tower leg, because of the sheltering effect from the windward tower leg and the transverse beams. The same observation is made for the lift coefficients of the leeward tower leg. The influence of the dummy deck segment on both the drag and lift coefficients of the leeward leg is also insignificant when $0^o \leq \beta_0 \leq 80^o$.

(3) The variation of the drag coefficient of the upper windward leg segment with yaw wind angle is very similar to that of the drag coefficient of the entire windward leg. The pattern of the drag coefficient of the lower windward leg segment is, however, slightly different from that of the upper windward leg segment. The drag coefficient of the lower windward leg segment is larger than that of the upper windward leg segment when β_0 is smaller than 75°.

(4) The variation of the drag coefficient of the upper segment of the leeward leg with β_0 is quite similar to that of the drag coefficient of the entire leeward leg. The variation of the drag coefficient of the lower segment of the leeward leg with β_0 is also similar to that of the drag coefficient of the entire leeward leg, except for β_0 larger than 70°. The drag coefficients of both upper and lower segments of the leeward leg are significantly different from those of the corresponding segments of the windward leg.

(5) The lift coefficients of the upper segments of both the windward and leeward tower legs, with and without the dummy deck segment, are very similar to those of the entire windward and leeward tower legs, respectively. The lift coefficients of the lower segment of the windward and leeward tower legs, however, are to a certain extent different from the above two cases.

(6) The variations of both drag and crosswind force coefficients with yaw wind angle are similar to each other for all the four transverse beams. The crosswind force coefficients vary with β_0 in a manner similar to a sine wave. The drag coefficient curves, however, seem to have the shape of a cosine wave but it is distorted in magnitude for β_0 ranging from 0° to 27° for the lower transverse beam, and from 0° to 15° for the other three transverse beams.

Acknowledgements

References

Boonyapinyo, V., Miyata, T. and Yamada, H. (1999), "Advanced aerodynamic analysis of suspension bridges by state-space approach", *J. Structural Engineering,* ASCE, **125**(12), 1357-1366.

Chen, X.Z., Matsumoto, M. and Kareem, A. (2000a), "Time domain flutter and buffeting response analysis of bridges", *J. Engineering Mechanics,* ASCE, **126**(1), 7-16.

Chen, X.Z., Matsumoto, M. and Kareem, A. (2000b), "Aerodynamic coupled effects on flutter and buffeting of bridges", *J. Engineering Mechanics,* ASCE, **126**(1), 17-26.

Davenport, A.G. (1962), "Buffeting of a suspension bridge by storm winds", *J. Structural Engineering*, ASCE, **88**(3), 233-268.

Diana, G., Bruni, S., Collina, A. and Zasso, A. (1998), "Aerodynamic challenges in super long bridges design", *Proc. of International Symposium on Advances in Bridge Aerodynamics,* Copenhagen, Denmark, May, 131-143.

Jain, A., Jones, N.P. and Scanlan, R.H. (1996), "Coupled buffeting analysis of long-span bridges", *J. Structural Engineering,* ASCE, **122**(7), 716-725.

Katsuchi, H., Jones, N.P. and Scanlan, R.H. (1999), "Multimode coupled flutter and buffeting analysis of the Akashi-Kaikyo bridge", *J. Structural Engineering*, ASCE, **125**(1)**,** 60-70.

Larose, G.L., Damsgaard, A., Diana G. and Falco, M., (1993), "Wind-tunnel investigations of the tower for the Stretto di Messina Bridge", *J. Wind Eng. Ind. Aerod.*, **48**, 379-393.

Larose, G.L., Falco, M. and Cigada, A. (1995), "Aeroelastic response of the towers for the proposed bridge over Stretto di Messina", *J. Wind Eng. Ind. Aerod.*, **57**, 363-373.

Larose, G.L., Zasso, A., Melelli, S. and Casanova, D. (1997), "Field measurements of the wind-induced response of a 254 m high free-standing bridge pylon", *2nd EACWE, Genova, Italy,* 1553-1560.

Lin, Y.K. (1979), "Motion of suspension bridges in turbulent winds", *J. Engineering Mechanics*, ASCE, **105**(6), 921-932.

Lin, Y.K. and Yang, J.N (1983), "Multimode bridge response to wind excitation", *J. Engineering Mechanics,* ASCE, **109**(2), 586-603.

Ricciardelli, F. and Vickery, B.J. (1998), "The aerodynamic characteristics of twin column, high rise bridge towers", *Wind and Structures*, **1**(3), 225-241.

Ricciardelli, F. and Vickery, B.J. (1994), "Wind loads on a pair of long prisms of square cross-section", *IN-VENTO-94, Proc. 3rd Nat. Italian Conf. Wind Engng., Roma,* October, 101-120.

Scanlan, R.H. (1978), "The action of flexible bridge under wind, II: buffeting theory", *J. Sound and Vibration*, **60**(2), 201-211.

Scanlan, R.H. and Gade, R.H. (1977), "Motion of suspension bridge spans under gusty wind", *J. Structural Engineering,* ASCE, **103**(9), 1867-1883.

Xu, Y.L., Sun, D.K., Ko, J.M. and Lin, J.H. (1998), "Buffeting analysis of long span bridges: a new algorithm", *Computers & Structures*, **68**, 303-313.

Xu, Y.L., Sun, D.K., Ko, J.M. and Lin, J.H. (2000), "Fully coupled buffeting analysis of Tsing Ma suspension bridge", *J. Wind Eng. Ind. Aerod.*, **85**(1), 97-117.

Zhu, L.D., Xu, Y.L. and Xiang, H.F. (2000), "Buffeting analysis of a long suspension bridge under inclined

wind", *Proc. of International Conference on Advances in Structural Dynamics*, Hong Kong, China, 13-15 December, **II**, 1535-1542.

Zhu, L.D., Xu, Y.L. Zhang, F. and Xiang, H.F. (2001), "Buffeting of a long suspension bridge: analysis and field measurement", *Proc. of SPIE 6th Annual International Symposium on NDE for Health Monitoring and Diagnostics*, Newport Beach, California, USA, March, 323-334.

CC